ACS NANO
Cite This: ACS Nano 2019, 13, 10074−10084
www.acsnano.org

ARTICLE

Thermoresponsive *in Situ* Forming Hydrogel with Sol−Gel Irreversibility for Effective Methicillin-Resistant *Staphylococcus aureus* Infected Wound Healing

Xu Yan,[†,#] Wei-Wei Fang,[†,#] Jingzhe Xue,[‡] Tian-Ci Sun,[†] Liang Dong,[‡] Zhengbao Zha,[§] Haisheng Qian,[§] Yong-Hong Song,[†] Min Zhang,[∥] Xinglong Gong,[‡] Yang Lu,[*,†] and Tao He[*,†]

[†]School of Chemistry and Chemical Engineering, Anhui Province Key Laboratory of Advanced Catalytic Materials and Reaction Engineering, Key Laboratory of Metabolism and Regulation for Major Diseases of Anhui Higher Education Institutes, Hefei University of Technology, Hefei, Anhui 230009, People's Republic of China

[‡]Department of Chemistry, Hefei National Research Centre for Physical Sciences at the Microscale, CAS Key Laboratory of Mechanical Behavior and Design of Materials, Department of Modern Mechanics, University of Science and Technology of China, Hefei 230026, People's Republic of China

[§]School of Food and Biological Engineering, Hefei University of Technology, Hefei, Anhui 230009, People's Republic of China

[∥]School of Life Science, Anhui University, Hefei, Anhui 230601, People's Republic of China

Supporting Information

ABSTRACT: **An *in situ* forming hydrogel has emerged as a promising wound dressing recently. As physically cross-linked hydrogels are normally unstable, most *in situ* forming hydrogels are chemically cross-linked. However, big concerns have remained regarding the slow gelation and the potential toxicity of residual functional groups from cross-linkers or the polymer matrix. Herein, we report a sprayable *in situ* forming hydrogel composed of poly(*N*-isopropylacrylamide$_{166}$-*co*-*n*-butyl acrylate$_9$)-poly(ethylene glycol)-poly(*N*-isopropylacrylamide$_{166}$-*co*-*n*-butyl acrylate$_9$) copolymer (P(NIPAM$_{166}$-*co*-nBA$_9$)-PEG-P(NIPAM$_{166}$-*co*-nBA$_9$), denoted as PEP) and silver-nanoparticles-decorated reduced graphene oxide nanosheets (Ag@rGO, denoted as AG) in response to skin temperature. This thermoresponsive hydrogel exhibits intriguing sol−gel irreversibility at low temperatures for the stable dressing of a wound, which is attributed to the inorganic/polymeric dual network and abundant coordination interactions between Ag@rGO nanosheets and PNIPAM. The biocompatibility and antibacterial ability against methicillin-resistant *Staphylococcus aureus* (MRSA) of this PEP-AG hydrogel wound dressing are confirmed *in vitro* and *in vivo*, which could transparently promote the healing of a MRSA-infected skin defect.**

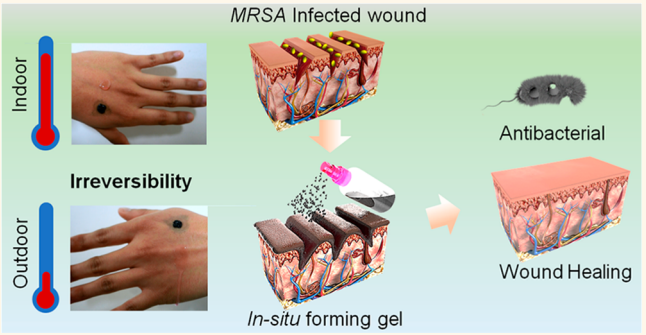

KEYWORDS: *hydrogel, in situ forming, sol−gel transition, irreversibility, wound closure, thermoresponsive, methicillin-resistant Staphylococcus aureus*

Hydrogels are basically 3-D cross-linked porous polymeric materials containing an abundant amount of water, with tunable mechanical properties.[1−4] There has been growing interest in the preparation of functional hydrogels with enhanced properties, together with various applications explored recently.[5−10] For example, with gold nanoparticles serving as multifunctional cross-linkers, a gold nanoparticle−PNIPAM nanocomposite hydrogel exhibited critical stress (1.02 MPa) and high toughness (7.1 MJ/m^3).[11] Very recently, a polyacrylamide (PAM)/aligned cellulose nanofibers (CNFs) hybrid hydrogel has been synthesized to mimic muscle; it exhibited a 500 times stronger tensile strength along the longitudinal direction compared with the general PAM hydrogel.[12] Guo *et al.* have fabricated a series of conducting injectable hydrogels with multifunctionality including drug release and antibacterial and antioxidant

Received: April 12, 2019
Accepted: August 20, 2019
Published: August 20, 2019

DOI: 10.1021/acsnano.9b02845
ACS Nano 2019, 13, 10074−10084

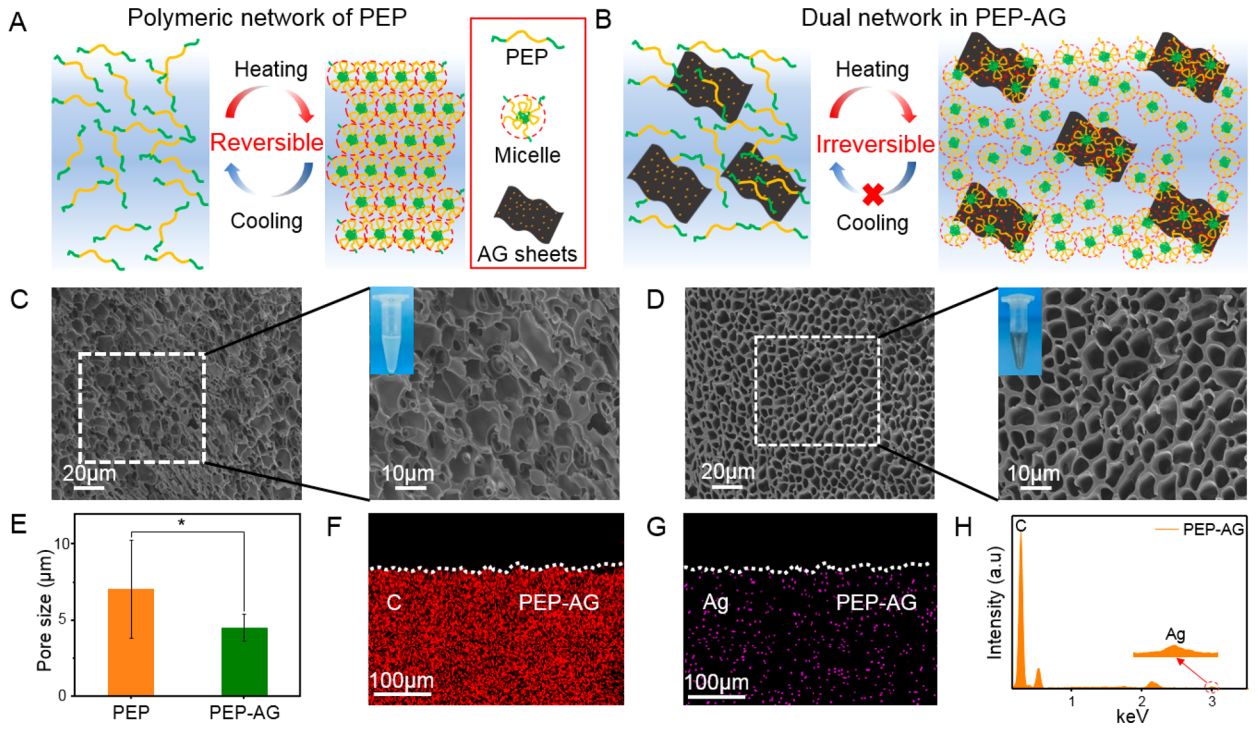

Figure 1. Characterization of PEP and PEP-AG hydrogels. Schematic structures in (A) the PEP hydrogel and (B) the PEP-AG composite hydrogel. Low- and high-resolution SEM images of porous structures in (C) the PEP hydrogel and (D) the PEP-AG hydrogel. (E) Pore size distributions of PEP and PEP-AG hydrogels. (F, G) EDS mapping of C and Ag elements in the PEP-AG hydrogel and (H) the relative spectrum.

activities, leading to the promotion of regeneration during wound healing.[13−15] Until now, as typical biocompatible materials, hydrogels have been widely applied in biomedicine including drug delivery and controlled release,[16,17] cell therapy and tissue engineering,[18−20] and oncology treatment.[21] More importantly, compared with conventional treatments for body wounds such as sutures, staples, and adhesive tapes, hydrogels could act as facilely and quickly applied barriers adhered onto a wet wound surface against microorganism penetration. They could form a moist environment and absorb excess exudates to accelerate the healing process, which can further deliver biocides to treat bacterial infections.[22−24]

Compared with preformed hydrogels, *in situ* forming hydrogels have emerged as promising wound dressing materials recently.[25,26] To be applied as efficient wound dressing materials, suitable *in situ* forming hydrogel candidates should possess several key features: (1) injectable and fast *in situ* gelation with great stability; (2) antibacterial, especially against drug-resistant bacterial such as MRSA; (3) clinically available.[27−29] Generally, two major processes have been employed in the *in situ* gelation: chemical and physical cross-linking, in which chemical reactions (such as Michael addition, click chemistry, Schiff base, enzyme-mediated, or photo-cross-linking reactions) or physical interactions have been employed to cross-link the networks, respectively.[30] However, chemical gelation mostly suffers from the addition of organic cross-linkers, which need to be stored separately and added into the matrix prior to the formation of the hydrogel. In some cases, external irradiation such as ultraviolet light is needed to initiate the cross-linking, resulting in practical inconvenience. The major concern that always remains is the potential cytotoxicity of the residual functional groups being used to build the highly cross-linked structures and the residual organic cross-linkers and catalyst.[31] In contrast, physically cross-linked hydrogels have been built *via* hydrogen bonding, chain entanglements, and coordination, which avoid the requirement of organic cross-linkers and exhibit promising compatibility. However, physically cross-linked hydrogels are mostly constrained by their instability, as they could partly or completely "switch back" to liquid in the absence of stimuli, leading to the failure of the wound dressing.[32,33] Therefore, stable physically cross-linked hydrogels are highly required for *in situ* forming wound dressing.

In wound care, methicillin-resistant *Staphylococcus aureus* (MRSA) infection is a big challenge in the clinic.[34] Despite the discovery of new formulas, synthetic organic antibiotics are weak against MRSA infection.[35] On the contrary, inorganic components such as silver nanoparticles exhibit promising inhibition against MRSA.[36] In view of developing a functional antibacterial hydrogel, we here report a thermoresponsive *in situ* forming irreversible hydrogel for effective MRSA-infected wound healing. As shown in Figure 1, Ag nanoparticle decorated reduced graphene oxide nanosheets (Ag@rGO, denoted as AG) with antibacterial activity have been incorporated into the poly(*N*-isopropylacrylamide$_{166}$-*co*-*n*-butyl acrylate$_9$)-poly(ethylene glycol)-poly(*N*-isopropylacrylamide$_{166}$-*co*-*n*-butyl acrylate$_9$) (denoted as PEP) copolymer scaffold to obtain a thermoresponsive PEP-AG hydrogel. Compared with traditional thermoresponsive hydrogels with reversible sol−gel and gel−sol transitions, this PEP-AG composite hydrogel shows an interesting sol−gel irreversibility after fast *in situ* forming on a skin wound. The PEP-AG hydrogel remains in a hydrogel state even at a low temperature of 5 °C, and the solid phase could be retained for at least 2 months. The irreversible gelation has been initiated by thermo-induced micelle packing of the block copolymers. The strong

DOI: 10.1021/acsnano.9b02845
ACS Nano 2019, 13, 10074−10084

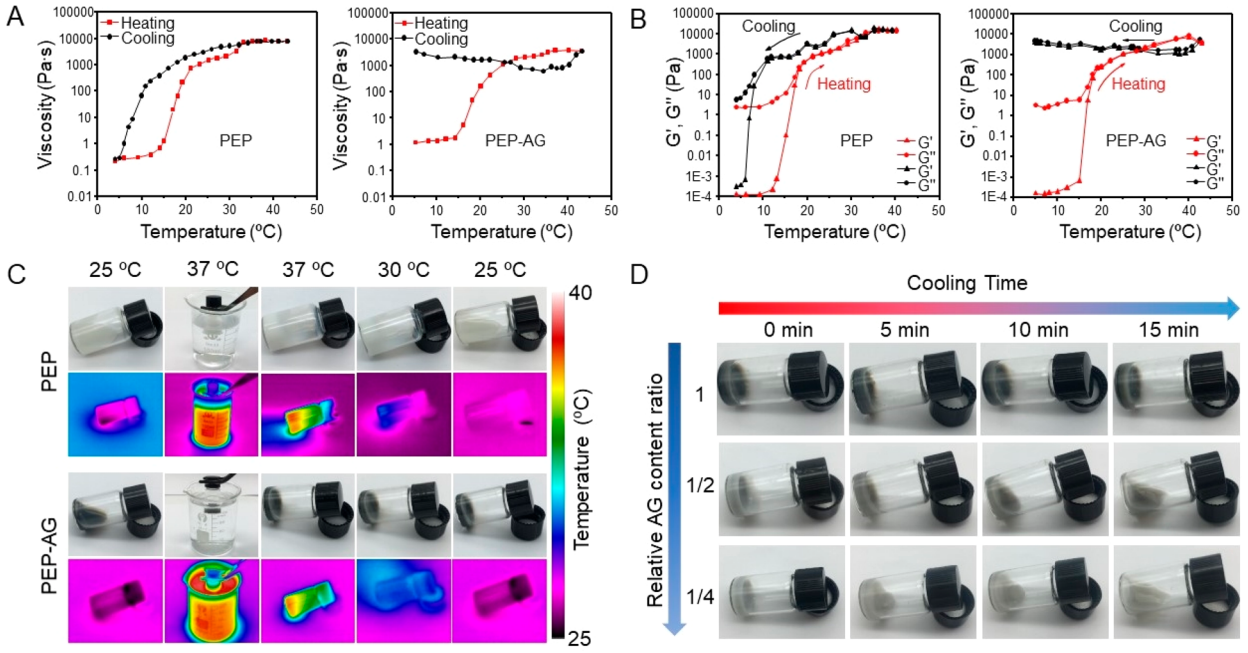

Figure 2. ***In situ*** **forming PEP-AG hydrogel with sol−gel irreversibility. (A) Viscosity measurements and (B)** G'/G'' **measurements of the PEP and the PEP-AG aqueous solution. (C) Digital pictures and infrared thermal images of PEP and PEP-AG aqueous solution under the heating−cooling process. (D) Digital pictures of PEP-AG hydrogels with different AG contents in a cold environment.**

synergistically coordination interactions between Ag@rGO nanosheets and the collapsed PNIPAM chains result in the enhanced stability against decreasing temperature. In combination with the biosafety and antibacterial property against MRSA, this irreversible hydrogel could be *in situ* formed immediately after a hybrid aqueous mixture is sprayed onto large-sized and deeply sharp skin wounds, which should contribute to a long-term wound dressing even outdoors in winter. Skin wound experiments confirmed this hydrogel could serve as an effective wound dressing to accelerate the healing of MRSA infection. Especially, this stable wound closure performance is required for an *in situ* forming physically cross-linked hydrogel in cold conditions especially alpine regions and high latitudes.

RESULTS AND DISCUSSION

Preparation of PEP-AG Thermoresponsive Composite Hydrogel. We employed biocompatible poly(*N*-isopropylacrylamide$_{166}$-*co*-*n*-butyl acrylate$_9$)-poly(ethylene glycol)-poly(*N*-isopropylacrylamide$_{166}$-*co*-*n*-butyl acrylate$_9$) (P(NIPAM$_{166}$-*co*-nBA$_9$)-PEG-P(NIPAM$_{166}$-*co*-nBA$_9$), $M_{n,\,GPC}$: 47k, PDI: 1.06) block copolymer to construct the thermoresponsive hydrogel polymeric matrix. PNIPAM was selected as a thermosensitive A block, while PEG served as a hydrophilic B block of copolymers. Generally, the low critical soluble temperature (LCST) of PNIPAM is around 32 °C. The introduction of hydrophilic PEG segments bestowed thermogelling properties to the polymer aqueous solution, but the subsequently increased LCST may be above body temperature. In order to respond to body temperature stimuli, we further copolymerized a small content of hydrophobic nBA with NIPAM to adjust the phase transition point below body temperature, and the obtained copolymer P(NIPAM$_{166}$-*co*-nBA$_9$)-PEG-P(NIPAM$_{166}$-*co*-nBA$_9$) exhibited promising gelling behavior. We denote this copolymer as PEP and used it during the rest of the experiments. The synthetic process and ^{1}H NMR spectra are shown in Figure S1 and Figure S2.

To introduce antibacterial activity to the PEP hydrogel, Ag@rGO nanosheets were homogeneously dispersed into the PEP polymer aqueous solution, and the weight ratio between Ag and rGO in the Ag@rGO nanosheets was determined to be approximately 5:4 by inductive coupled plasma atomic emission spectrometry (ICP-AES) and thermogravimetric analysis (TGA) (SI, Figures S3 and S4). The composite hydrogel could form immediately when the temperature of the mixture dispersion was increased above 30 °C (SI, Figure S5, Movie S1 and S2), which was a little lower than skin temperature. The addition of Ag@rGO nanosheets (0.75 wt %) did not affect the thermal responsivity of the PEP hydrogel. Typical porous structures in PEP and PEP-AG were shown in the SEM images (Figure 1C,D). According to these SEM images, the average pore diameters of PEP and PEP-AG hydrogels were measured to be 7.06 ± 3.25 μm and 4.51 ± 0.87 μm, respectively (Figure 1E), indicating the neatly ordered and smaller-sized pores in the PEP-AG hydrogel. The presence of Ag@rGO nanosheets in the PEP-AG hydrogel could be observed in the TEM image of a lyophilized sample (SI, Figure S6). In the UV−vis spectrum of the PEP-AG composite hydrogel, the absorption peak around 400 nm corresponded to the surface plasmon resonance of Ag nanoparticles (SI, Figure S7). As shown in Figure S8, the X-ray diffraction (XRD) patterns of the AG nanosheets and PEP-AG hydrogel are in good agreement with the face-centered cubic standard of silver crystal structure (JCPDS No. 04-0783). Energy dispersive spectroscopy (EDS) elemental mapping images directly showed the uniform distribution of Ag@rGO nanosheets in the obtained PEP-AG hydrogel (Figure 1F−H).

In Situ **Forming PEP-AG Hydrogel with Sol−Gel Irreversibility.** The PEP copolymer in aqueous solution exhibited typically a thermally sensitive sol−gel transition.

DOI: 10.1021/acsnano.9b02845
ACS Nano 2019, 13, 10074−10084

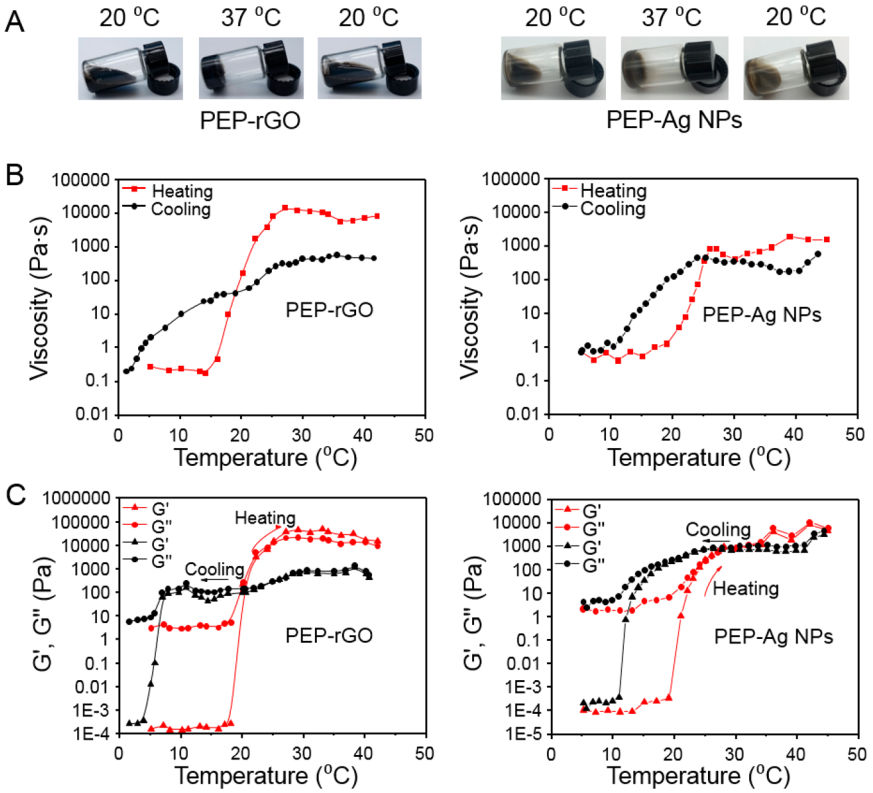

Figure 3. Reversibility of PEP-rGO and PEP-Ag NPs hydrogels at low temperatures. (A) Digital pictures, (B) viscosity, and (C) G'/G'' measurements of PEP-rGO and PEP-Ag NPs aqueous dispersions in the heating−cooling process.

When the temperature was increased, the PNIPAM chain of the PEP hydrogel collapsed and subsequently formed the hydrophobic species. This could be attributed to the breaking of hydrogen bonds between PNIPAM and water on increasing the temperature. Meanwhile, the PEG chains served as the bridges to cross-link adjacent hydrophobic species. The formed PEP hydrogel was observed to switch back to solution with decreasing the temperature from 37 °C to 25 °C. In this liquidation process, PNIPAM could turn back to being hydrophilic at a low temperature (<LCST), and the aggregation of hydrophobic species may disassemble at the same time (Figure 1A).

However, the formed PEP-AG thermoresponsive composite hydrogel would not switch back to liquid even when the temperature was cooled to as low as 5 °C (Figure 2). As shown in digital photos and infrared thermal images (Figure 2C), this irreversibility of the PEP-AG hydrogel in response to cooling stimuli could be directly observed. Both PEP and PEP-AG aqueous solutions exhibited a sol−gel phase transition after being immersed in a water bath at 37 °C. After removing the water bath, the PEP-AG hydrogel still retained its gel state at ambient temperature (~20 °C), while the PEP hydrogel could not maintain its shape and finally dissolved into a liquid.

Rheological properties of PEP and PEP-AG hydrogels were measured to investigate the mechanism of the irreversibility of the PEP-AG hydrogel (Figure 2A,B). The storage and loss modulus (G' and G'' data) curves of the PEP hydrogel were separated with decreasing temperature from 37 °C to 20 °C. In contrast, G' and G'' data curves of the PEP-AG hydrogel were not separated from each other (Figure 2B). After approaching the maximum value at around 35 °C, the viscosity data remained as almost a constant, no matter when the temperature was cooled to 5 °C, which indicated that the formed PEP-AG hydrogel was stable on decreasing the temperature (Figure 2A). Compared with the reversible PEP hydrogel, the irreversibility property of the PEP-AG hydrogel was confirmed to be attributed to the addition of Ag@rGO nanosheets.

To further investigate the mechanism of the irreversibility property observed in the PEP-AG hydrogel, thermoresponsive PEP-AG hydrogels with lower contents of Ag@rGO nanosheets have been fabricated as control samples, including PEP-$AG_{1/2}$ (half content of AG sheets) and PEP-$AG_{1/4}$ (a quarter content of Ag@rGO nanosheets), which were reversible to the solution at low temperature (Figure 2D). Therefore, the irreversibility of PEP-AG hydrogels was revealed to be AG concentration dependent, as enough Ag@rGO nanosheets were required to form a stable dual network in the composite hydrogel. In addition, a series of PEP hydrogels composed of only Ag nanoparticles (denoted as PEP-Ag NPs hydrogel) or bare rGO nanosheets (PEP-rGO hydrogel) have been prepared in related control experiments (Figure 3). Both these PEP-Ag NPs and PEP-rGO hydrogels could be reversible to liquid at a low temperature, and the typical sol−gel and consequent gel−sol transitions have been observed in the heating−cooling cycle (Figure 3B,C).

According to the above results from the PEP-AG hydrogel and a series of control samples, the proposed formation of the stable dual network in the irreversible PEP-AG hydrogel is shown in Figure 1B. The addition of 2D materials such as GO nanosheets could form a dual network in a composite hydrogel without any organic cross-linker.[9,37] In the as-prepared PEP-AG composite hydrogel, the presence of a Ag−amino coordination interaction was revealed by FT-IR data (SI,

DOI: 10.1021/acsnano.9b02845
ACS Nano 2019, 13, 10074−10084

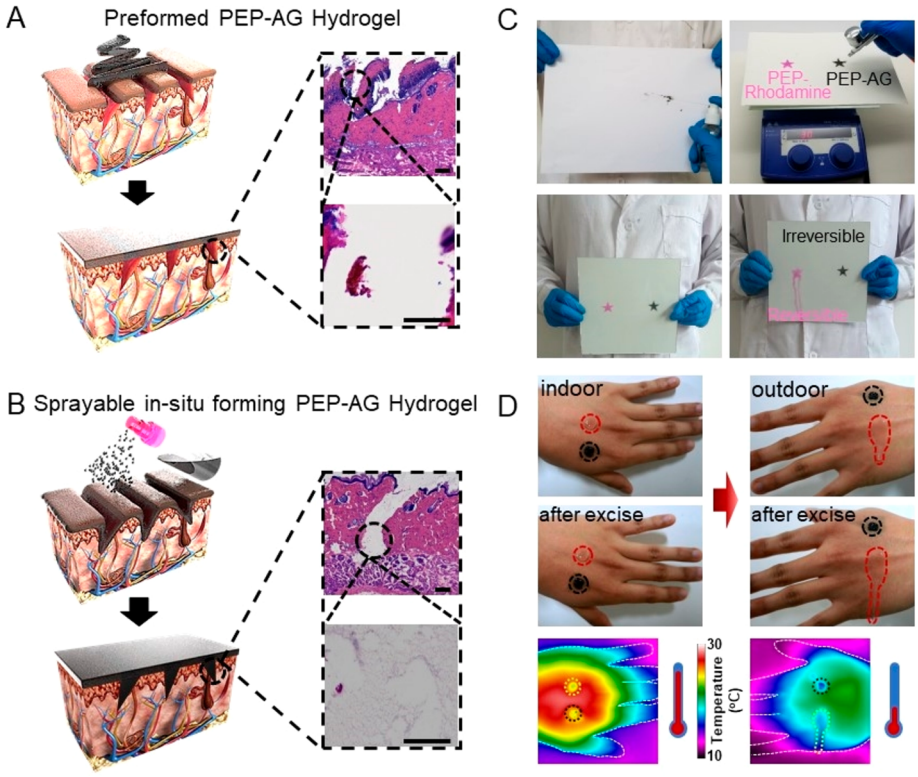

Figure 4. Sprayable and irreversible *in situ* forming PEP-AG hydrogel as a stable wound dressing. Deep and sharp wound areas being treated by (A) preformed PEP-AG hydrogel and (B) sprayable *in situ* forming PEP-AG hydrogel. Inset: Filling effects shown in H&E histological slices. Scale bar: 200 μm. Zoomed-in region, scale bar: 50 μm. (C) Sprayable *in situ* formation process of the PEP-AG hydrogel with complex shapes on a heated silica gel plate at 30 °C, maintaining the shape after removing the heater, while the rhodamine-containing PEP hydrogel (PEP-rhodamine) switches back to a liquid in a cold environment. (D) Digital pictures and infrared thermal images of the reversible rhodamine-PEP hydrogel and irreversible PEP-AG hydrogel on human hand skin indoors (warm) and outdoors (cold) in winter.

Figure S9). As a result, in the heating process, Ag@rGO nanosheets served as both the building blocks for an inorganic scaffold and the cross-linkers attributed to Ag−amino coordination bonding. Individual PNIPAM chains in the same hydrophobic species could interact with Ag nanoparticles on different Ag@rGO nanosheets, and the linkages also occur among adjacent PEP hydrophobic species *via* Ag@rGO nanosheets. Compared with PEP, PEP-Ag NPs, and PEP-rGO hydrogels, the strong connections between Ag@rGO nanosheets and PEP hydrophobic species obviously reinforced the physically cross-linked PEP-AG hydrogel, which contributed to the irreversibility in the cooling cycle. In addition, the reversible PEP-AG hydrogels with half and a quarter AG contents further confirmed the contribution of the dual network.

Hydrogels-based wound dressings should have great mechanical properties to satisfy the requirement of human soft tissue.[13] Herein, the mechanical performances of a series of PEP-AG hydrogels with varying AG content were investigated. As shown in Figure S10A, the tensile strength of the composite hydrogel gradually increased with the increasing content of AG from 0.25 wt % to 0.75 wt %. The tensile stress of the PEP-AG (0.75 wt %) hydrogel reached 161 kPa, which was 4.2 times that of the pure PEP hydrogel. However, when the AG content reached 1 wt %, the tensile strength of the hydrogel sharply decreased owing to the poor dispersion of excessive amounts of Ag@rGO nanosheets in PEP solution. The Young's modulus of the composite hydrogels indicates a similar trend to the tensile strength, and the PEP-AG (0.75 wt %) hydrogel exhibits an optimized modulus (4.058 MPa) (Figure S10B).

Sprayable *in Situ* Forming PEP-AG Hydrogel as an Irreversible Wound Dressing. The hydrogel dressing could maintain a considerable moist wound environment to absorb tissue surplus exudates.[15,38] Due to the quick response to body temperature stimuli and sharply swelling (ESR = 43), the PEP-AG hydrogel could be applied as an *in situ* forming wound dressing. In view of the low viscosity of the original aqueous composite solution, it could not only be smeared onto the skin wound area but also be facilely sprayed to form a hydrogel dressing *in situ*. The sprayable and thermally responsive features of the PEP-AG hydrogel are potentially useful in some special treatments such as large-area burn wound care, where injectable preformed hydrogels could not easily cover the whole wound area.[25] When being sprayed onto an animal skin wound area, only a small amount of the precursor aqueous dispersion was needed, and the wound area was more homogeneously covered by the subsequently quickly formed hydrogel compared with the injected ones. More importantly, compared with traditional hydrogels, this sprayable *in situ* forming PEP-AG hydrogel exhibited an advantage in deeper penetration for deep and sharp wounds (Figure 4A,B). In the hematoxylin and eosin (H&E) histological images of this sharp wound after treatment with the PEP-AG spray, the deep region in the lesion was filled with the hydrogel (Figure 4B).

As shown in Figure 4C, the PEP-AG mixture could be facilely sprayed onto varied substrates such as a heated silica gel plate at 30 °C to form a hydrogel *in situ*. The shape was

DOI: 10.1021/acsnano.9b02845
ACS Nano 2019, 13, 10074−10084

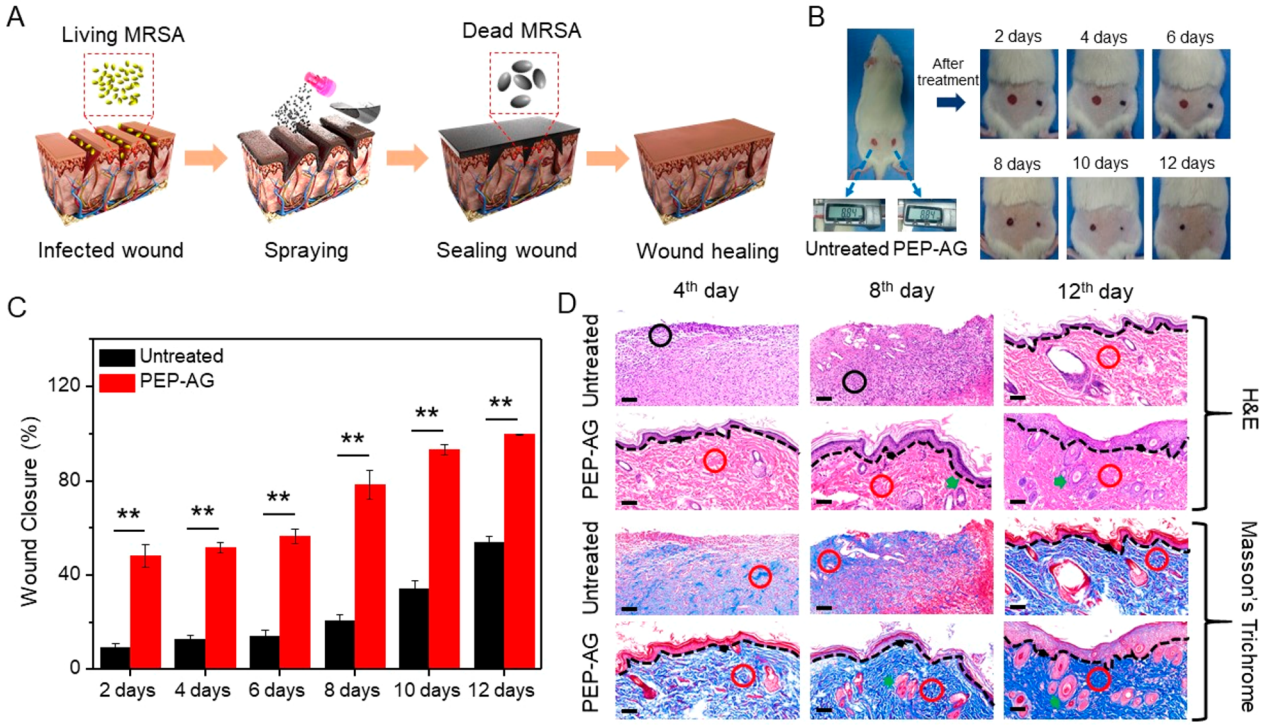

Figure 5. PEP-AG hydrogel-accelerated healing of a MRSA-infected wound on rats. (A) Illustration of the PEP-AG hydrogel as an antibacterial dressing by spray procedure onto the MRSA-infected wound. (B) Two round MRSA-infected wounds were made on the two sides of depilated back skin of the hip on each rat. The left wound remained untreated, while the right wound was covered by the PEP-AG hydrogel, and pictures were collected on the second, fourth, sixth, eighth, 10th, and 12th days in the wound healing process. (C) Wound closure rate in untreated group and PEP-AG group (error bars are standard deviation, $n = 5$). (D) Pathological examination of a skin section collected from the wound areas in the untreated group and PEP-AG group on the fourth, eighth, and 12th days. Black circle, red circle, black arrow, green arrow, and black dashed line indicate inflammatory cells, collagen fibers, epidermis, hair follicles, and boundary of epithelium and dermis, respectively. Scale bar: 100 μm.

controllable with the assistance of a mask in the spraying process. The PEP hydrogel could also be sprayed onto the skin wound area in response to body temperature. However, the reversible feature of the PEP hydrogel would result in the failure of closure of the wound after exposure to a cold outdoor environment. In comparison, the PEP-AG hydrogel formed on a silicon plate could maintain a five-pointed-star shape under an ambient temperature of around 20 °C, while the PEP hydrogel transited to a liquid after removal of the heat source (Figure 4C). The irreversibility of the PEP-AG hydrogel was highly useful for the quick treatment of skin wounds, especially in cold conditions including alpine regions and high latitudes. A study on human skin further confirmed this benefit of the irreversible PEP-AG hydrogel (Figure 4D). The significant difference between PEP and PEP-AG hydrogels in a cold outdoor environment around 10 °C could be directly observed in digital photos and infrared thermal images. The PEP-AG hydrogel could keep a stable shape and adhere onto hand skin during winter outdoor exercise, where the temperature was around 10 °C, while the PEP hydrogel transited to a fluid and then almost drained off the skin (Figure 4D and Movies S3 and S4).

Infected Skin Wound Healing Using Irreversible PEP-AG Hydrogel. Hydrogels used in wound management need to possess antibacterial activity to prevent infections and to accelerate the healing process.[22] Here, we evaluated this property according to inhibition zones. We prepared the stable PEP-AG hydrogel by heating the hybrid solution and then cooling it to room temperature. As shown in Figure S11, the inhibition zones around the PEP-AG hydrogel against methicillin-resistant *Staphylococcus aureus* (MRSA) and *Escherichia coli* (*E. coli*) were 1.3 and 1.4 cm, respectively, which indicated the promising antibacterial activities of the PEP-AG hydrogel comparable to the Ag nanoparticles-containing hydrogel (PEP-Ag NPs). In contrast, inhibition zones were absent in both the PEP and PEP-rGO hydrogels groups. As the broad antibacterial activity and mechanism of silver nanoparticles have been deeply studied,[39] the antibacterial activity could be ascribed to the Ag nanoparticles loaded on the rGO nanosheets. Moreover, in order to investigate the anti-MRSA infection performance and healing rate of the PEP-AG hydrogel *in vivo*, we performed a skin wound healing evaluation on Sprague−Dawley (SD) rats (Figure 5A,B). A PEP-AG aqueous dispersion was sprayed onto a wound on the right side of each rat, while the left wound remained untreated as a control. After spraying, the PEP-AG composite hydrogel could form *in situ* quickly to cover the damaged skin area in response to the local skin temperature, and no additional cross-linker or external stimuli such as NIR and UV light was required. Notably, this irreversible hydrogel stayed on the wound area firmly and would not switch back to liquid even if the environmental temperature decreased. As shown in Figure 5B, the PEP-AG-treated group (right) exhibited obviously accelerated wound healing and epidermis regeneration in comparison with the MRSA-infected control group (left). The wound suffering from the MRSA infection was difficult to heal. It could be observed that only 54% of wound areas were closed in the untreated group after 12 days. In comparison, the wound

DOI: 10.1021/acsnano.9b02845
ACS Nano 2019, 13, 10074−10084

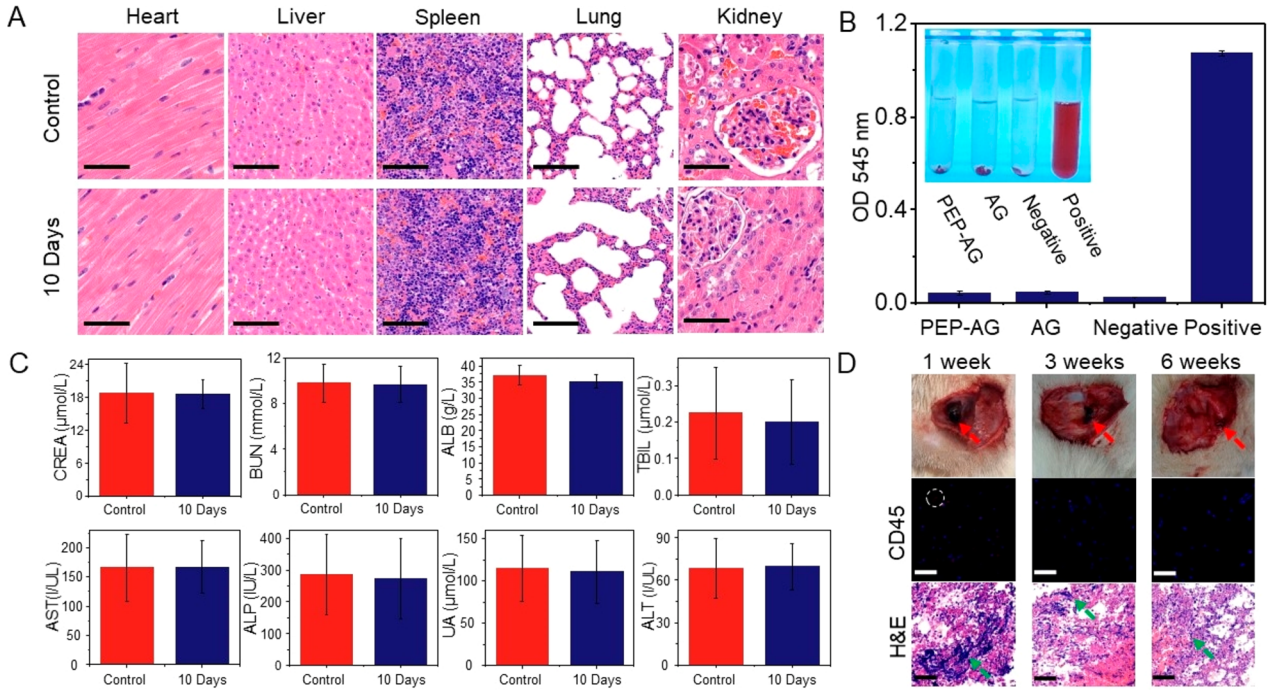

Figure 6. PEP-AG hydrogel-accelerated healing of MRSA-infected wounds on rats. (A) H&E-stained tissue sections from major organs in rats 10 days after the subcutaneous administration of PEP-AG hydrogel. Scale bar: 20 μm. (B) Hemolysis evaluation of the PEP-AG hydrogel. (C) Evaluation of liver and kidney function of rats 10 days after the administration of the PEP-AG hydrogel (n = 5). (D) Compatibility and degradability test of subcutaneously injected PEP-AG hydrogel at 1, 3, and 6 weeks postinjection. In digital pictures, and immunofluorescent (CD45) staining and H&E staining images of PEP-AG and its surrounding tissue, red and green dashed arrows indicate the location of the hydrogel, and the white circular region indicates leucocytes. Scale bar: 50 μm.

closure ratio in the PEP-AG hydrogel group was much faster, and 99.85% of the infected wound areas were healed after 12 days (Figure 5C).

MRSA bacterial colonies were found on agar plates corresponding to the wounds on the two sides at 2 h postinfection (SI, Figure S12), which indicated the successful construction of the MRSA-infected wound model on rats before wound care. To investigate the anti-infection efficacy of the PEP-AG hydrogel at 12 days post-treatment, the swab samples collected from the infected skin wounds were diluted and cultured on Luria−Bertani (LB) agar plates. Compared with the untreated control group, there were few bacterial colonies on the plate after 12 days in the PEP-AG group, which suggested the good recovery against infection (SI, Figure S12). Wound healing is an integral process of tissue growth and regeneration, which includes hemostasis, inflammation, migration, proliferation, and maturation.[40] Here, we performed H&E and Masson's Trichrome staining to evaluate the wound healing progress. As shown in Figure 5D, on the fourth day, a large number of inflammatory cells and few collagen fibers were observed in the untreated group. Compared with the untreated group, the basic structure of epithelium and abundant collagen fibers were observed in wounds of the PEP-AG group, and inflammatory cells were rarely observed. On the eighth day, although a few collagen fibers formed in the wounds of the untreated group, a large number of inflammatory cells were still present and no regeneration of epithelium was observed. However, the PEP-AG group showed high regularity of both epithelium and connective tissue with more fibroblasts and epithelium structure on the eighth day. On the 12th day, a thin epidermis and more collagen fibers formed in the untreated group, but the collagen fibers displayed a loose reticular arrangement, and the space between the collagen was large. On the contrary, complete epidermis and a higher regularity collagen fiber structure formed in wounds of the PEP-AG group, which were almost the same as normal skin tissues. Particularly, the appearance of mature hair follicles further proved the promotion during wound healing in the PEP-AG hydrogel group.

***In Vitro* and *in Vivo* Biocompatible Evaluation.** The cytotoxicity of the PEP-AG hydrogel has been evaluated on human umbilical vein endothelial cells (HUVEC) by a standard MTT study. The cell viability was over 98% even at a high concentration of 200 μg/mL, exhibiting a good cellular compatibility (SI, Figure S13A). Moreover, the long-term cytotoxicity evaluation of the PEP-AG hydrogel was performed on NIH-3T3 mouse embryo fibroblast cells, indicating no obvious inhibition of growth in 3 days at a concentrations from 50 to 200 μg/mL (SI, Figure S13B,C). Histological assessment of tissue containing representative organs including heart, liver, spleen, lung, and kidney has also been performed to evaluate long-term biocompatibility of the PEP-AG hydrogel (Figure 6A). In H&E staining images of the PEP-AG group, no obvious histopathological abnormality or lesion was observed. In addition, red blood cells of rabbit were exposed to our PEP-AG hydrogel, and no hemolysis was induced (Figure 6B). To further investigate the long-term biocompatibility of the PEP-AG hydrogel, serum biochemistry tests on rats were performed after 10 days of subcutaneous injection, and the major indexes of kidney and liver functions remained in the normal range, indicating no severe damage caused by the composite hydrogel (Figure 6C).

To quantitatively evaluate the stability of the hydrogel, the *in vitro* weight remaining ratio was recorded, and PEP-AG

DOI: 10.1021/acsnano.9b02845
ACS Nano 2019, 13, 10074−10084

hydrogels with different AG contents exhibited obvious mass losses after 30 days of incubation (SI, Figure S14). Moreover, a gross examination was performed to evaluate the degradation of the as-prepared hydrogel *in vivo*. The PEP-AG hydrogel remained intact within 1 week of postinjection. Then the hydrogel decomposed after 3 weeks, followed by complete dissociation after 6 weeks (Figure 6D). The residue weight of the PEP-AG hydrogel decreased with time (SI, Figure S15A), and the deformation of the porous structure could be observed (SI, Figure S15B), corresponding with observation from digital images in Figure 6D. H&E staining and immunohistochemical staining (anti-CD45 antibody) were further employed to identify inflammatory cells in tissues surrounding the injected hydrogels (Figure 6D). Immunofluorescence staining results suggested that there were few CD45 cells after 6 weeks, indicating only weak inflammatory response to the PEP-AG hydrogel.

CONCLUSIONS

In summary, we prepared a thermoresponsive *in situ* forming irreversible hydrogel, which was composed of a copolymer of PEP and Ag@rGO nanosheets. The aqueous PEP and Ag@rGO nanosheets could transit immediately to the hydrogel in response to an increasing temperature of about 30 °C. The skin temperature is higher than this responsive temperature, so this PEP-AG composite hydrogel could serve as a skin-temperature-responsive *in situ* forming wound dressing, and the addition of Ag@rGO nanosheets does not change the thermal response of the PNIPAM-based PEP hydrogel in the sol−gel transition. As a physically cross-linked hydrogel, there is no guest organic cross-linker, which rules out the potential toxicity from residual functional groups used for chemical cross-linking. Moreover, as an *in situ* forming hydrogel, this PEP-AG hydrogel could be administered by spraying the hybrid aqueous mixture onto the targeted skin area. Compared with the smearing of preformed hydrogels, this sprayable PEP-AG hydrogel is conducive to the careful treatment of patients with large-area burns, as well as deep penetration into sharp wound gaps to completely seal the wound, leading to sutureless repair and the promotion of healing. Typically, a physically cross-linked PNIPAM thermal responsive hydrogel such as PEP hydrogel would transit back to solution at low temperatures. Here, with the incorporation of Ag@rGO nanosheets into the micelle network of the PEP hydrogel, there are abundant coordination interactions between silver nanoparticles decorated on rGO nanosheets and amino groups in the collapsed PNIPAM chain in the formed inorganic/polymeric dual network. As a result, the obtained PEP-AG hydrogel is endowed with promoted stability in chilly conditions, which is irreversible to a liquid even at 5 °C, as suggested by rheometer measurements. As comparison samples, PEP composite hydrogels incorporated with only silver nanoparticles (PEP-Ag NPs hydrogel) or only rGO nanosheets (PEP-rGO hydrogel) show similar reversible gel−sol transition of the PEP hydrogel at room temperature, which further demonstrates the crucial contribution of Ag@rGO nanosheets. In combination with the sprayable and *in situ* forming features, the irreversibility further confirms the PEP-AG hydrogel could serve as a more stable and suitable wound dressing in cold weather and in alpine regions and high latitudes. In addition, cellular toxicity, biochemical and histological evaluation, and degradation experiments *in vivo* confirmed the biocompatibility of the PEP-AG hydrogel. As a stable wound dressing, this Ag nanoparticle-containing PEP-AG hydrogel shows excellent antibacterial property against MRSA, leading to an obvious acceleration of MRSA-infected wound healing in 2 weeks compared with untreated wounds.

MATERIALS AND METHODS

Materials. Except for the purification of nBA and NIPAM to remove the inhibitor, all chemical reagents were purchased and used without further treatment.

Preparation of PEP Copolymers. The PEP copolymers were synthesized by atom transfer radical polymerization (ATRP) in the presence of the macroinitiator (Br-PEG-Br).[41] Briefly, 2-bromo-2-methylpropionyl bromide (3.4 g, 14.8 mmol), PEG (15.0 g, 3.75 mmol, 4 kDa), and triethylamine (1.8 g, 17.8 mmol) were dissolved in dichloromethane (150 mL) and stirred in an ice bath for 72 h under N_2. The solution was then dialyzed followed by freeze-drying to offer the macroinitiator as a white solid. Typical polymerization was as follows: NIPAM (2.5 g, 22.1 mmol), nBA (0.16 g, 1.2 mmol), CuCl (28.6 mg, 0.3 mmol), and macroinitiator (0.21 g, 0.05 mmol) were dissolved in isopropanol/water (95/5 by w/w %). After deoxygenation, Me_6TREN (80.3 mg, 0.36 mmol) was introduced *via* microsyringe, and the polymerization was conducted for 72 h at room temperature. The reaction was stopped (conversion 75%), and the final product, poly(*N*-isopropylacrylamide$_{166}$-*co*-*n*-butyl acrylate$_9$)-poly(ethylene glycol)-poly(*N*-isopropylacrylamide$_{166}$-*co*-*n*-butyl acrylate$_9$), could be obtained as a white solid after passing the reaction mixture through aluminum followed by precipitation in cold *n*-hexane.

Synthesis of Ag Nanoparticles, rGO-PSS, and Ag@rGO Nanosheets. Poly(sodium 4-styrenesulfonate) (PSS)-stabilized rGO nanosheets (denoted as rGO-PSS) and Ag nanoparticle-decorated reduced graphene oxide nanosheets (Ag@rGO, denoted as AG) were synthesized according to our previous reports.[42] Ag nanoparticles were prepared according to a previous report by Hu *et al.*[43] Briefly, GO was reduced to rGO using hydrazine hydrate as reductant. Afterward, the rGO-PSS solution was prepared and kept at 60 °C. The $AgNO_3$ solution was added into the rGO-PSS solution using a double-jet pump at a speed of 0.5 mL h^{-1}. Finally, the Ag@rGO nanocomposite was obtained after washing and diluting with deionized water.

Preparation of the Composite Hydrogel. To prepare the PEP hydrogel, PEP polymers dissolved in saline solution (25 wt %) were taken out of a 4 °C refrigerator, followed by immersion in hot water or placing on a heater. For the PEP-AG composite hydrogel, Ag@rGO nanosheets were added into the PEP saline solution at a final concentration of 0.75 wt %, followed by heating. To investigate the contribution of AG concentration, PEP-AG$_{1/2}$ and PEP-AG$_{1/4}$ composite hydrogels with 1/2 and 1/4 content of Ag@rGO nanosheets were obtained to compare with the PEP-AG hydrogel. In addition, two control samples (PEP-Ag NPs hydrogel and PEP-rGO hydrogel) were prepared in a similar process by replacing Ag@rGO nanosheets with Ag nanoparticles and rGO-PSS nanosheets. The obtained hydrogel samples were freeze-dried for further characterizations.

Formation of Sprayable and Irreversible Hydrogel. To observe the phase transition of the PEP hydrogel on substrate and skin, rhodamine dye was mixed with PEP solution to prepare a PEP-rhodamine hydrogel. PEP-rhodamine (25 wt %) and PEP-AG (25 wt %) aqueous mixtures were sprayed onto a heated silicon plate at 30 °C, respectively, with the assistance of a five-pointed-star-shaped mask. After around 30 s, both PEP-rhodamine and PEP-AG hydrogels were formed *in situ* on the heated silicon plate after a typical thermally responsive sol−gel transition. To further investigate the stability of the *in situ* formed hydrogels, the heated silicon plate was removed from the heater (IKA, German), and the temperature was decreased to about 20 °C. Photo and thermal images of the phase transition in this heating−cooling cycle were recorded. To further investigate the formation of this irreversible PEP-AG hydrogel *in situ* on human skin, 200 μL of PEP-rhodamine (25 wt %) and PEP-AG (25 wt %) aqueous mixtures were dropped onto the hand back in warm indoor

DOI: 10.1021/acsnano.9b02845
ACS Nano 2019, 13, 10074−10084

conditions, and the hand with *in situ* formed hydrogels was rolled repeatedly. Then the hand with hydrogels was moved to a cold outdoor environment (<10 °C) in winter for 15 min, followed by repeated rolling. Infrared thermal images and videos of the hydrogels on the hand were recorded.

Sample Characterizations. ^{1}H NMR spectra were recorded from an Agilent VNMRS600 instrument. Fourier transform infrared spectroscopy (FT-IR) was performed on a Thermo Nicolet 67. Scanning electron microscopy (SEM) was performed on a Zeiss Supra 40, and transmission electron microscopy (TEM) was performed on a Hitachi HT7700. Constituent elements of the samples were analyzed by EDS (X-Max, Oxford). XRD was measured by a Philips X'Pert PRO SUPER X-ray diffractometer. UV−visible spectra of PEP and Ag@rGO aqueous mixtures were recorded using a Shimadzu UV-2600 spectrometer. A Fluke Ti400 infrared thermal imaging system was used. Triple detection (refractive index, multiangle-laser-light scattering, and viscosity) gel permeation chromatography (GPC) (Agilent PL-GPC 50) was utilized to measure the absolute number molecular weights and the polydispersities of the polymers. Viscosity and storage/loss modulus (G'/G'') were recorded using an Anton Paar MCR302 rheometer equipped with a 20 mm parallel-plate configuration.

Antibacterial Activity Evaluation. MRSA (Mu50) and *E. coli* (DH5α) were employed to evaluate the antibacterial effect of the samples including PEP-AG, PEP, PEP-Ag NPs, and PEP-rGO hydrogels. A 100 μL diluted bacterial suspension (10^6 CFU/mL) was spread onto LB agar plates uniformly. Then, preformed hydrogel samples with a diameter of 0.3 cm were placed onto agar plates with *E. coli* and MRSA, respectively. Antibacterial effects of these samples were evaluated by measuring the diameters of inhibition zones after incubation at 37 °C for 24 h.

Wound Penetration Test. SD rats (220 g, male) were chosen for the wound penetration test. After anesthetizing the rats by intraperitoneal injection of chloral hydrate (10%, 0.3 mL per 100 g bodyweight), hair-shaved areas (about 3 × 3 cm^2) were disinfected with 75% alcohol, and a laceration on the epidermis of rats was made using sterile syringe needles. The wounds were covered by preformed hydrogel and sprayable *in situ* forming hydrogel, respectively. After 24 h, the treated skin region was collected for histological analysis (H&E staining).

MRSA-Infected Wound Healing Experiment. Five SD rats in each experimental group were used for the wound healing test (n = 5). After anesthetizing the rats by intraperitoneal injection of chloral hydrate (10%, 0.3 mL per 100 g bodyweight), the dorsal hair was shaved. Then, two full-thickness round skin wounds with a diameter of approximately 0.8 cm were made on each side of depilated back skin of the hip on each rat. To construct a MRSA-infected wound model, an aliquot of MRSA suspension (100 μL, 10^6 CFU/mL) was inoculated onto each skin wound area. Sterilized cotton swabs were employed to collect bacterial samples from the surface of wound sites at 2 h postinfection (just before hydrogel dressing) and 12 days post-treatment. Then, the collected swabs were put into normal saline solution (0.5 mL), and the viable MRSA loads in the diluted bacterial suspensions were pilot studied by the instantly streaking plating method on LB agar plates for 24 h at 37 °C. The irreversible PEP-AG hydrogel was formed and covered onto the right wound on each rat, while the left wound remained untreated. A Vernier caliper was used to measure the area of the infected wound at 2, 4, 6, 8, 10, and 12 days post-treatment. The wound closure was calculated according to the following equation: wound closure (%) = $[W_0 - W_n]/W_0 \times 100\%$, where W_0 and W_n (n = 2, 4, 6, 8, 10, 12) represent the wound areas on day 0 and the second, fourth, sixth, eighth, 10th, and 12th days, respectively. H&E and Masson's Trichrome staining were used to evaluate the wound healing process. All the animal experimental protocols were approved by the Institutional Animal Care and Use Committee (IACUC) of Anhui Medical University (LLSC20150134).

Toxicity Evaluation of PEP-AG Hydrogel. Cytotoxicity of the PEP-AG hydrogel was evaluated on HUVEC and NIH-3T3 mouse embryo fibroblast cells by standard MTT assay and AO-EB staining. Cells were exposed to PEP-AG with varying concentrations from 50 to 200 μg/mL (n = 3). The hemolytic potential of the PEP-AG hydrogel was further measured using rabbit blood.[44] Typically, 0.1 mL of anticoagulated rabbit blood was added to 5 mL of distilled water (positive control), normal saline (negative control), and normal saline containing 10 mg of hydrogel followed by incubation at 37 °C for 1 h, and the optical densities at 545 nm of the collected supernatants were measured. A 0.5 mL amount of PEP-AG preformed hydrogel was subcutaneously injected by a syringe (23-gauge needle) for the toxicity evaluation on a rat. To evaluate the potential organ damage, histological analysis (H&E staining) of the major organs (heart, liver, spleen, lung, and kidney) was performed on SD rats 10 days postinjection of PEP-AG hydrogel. At the same time, the blood samples were collected in the PEP-AG group and normal rats for biochemical index evaluation.

Statistical Analysis. Mean values, standard deviations, and p-values were calculated in OriginPro 8.0. The experimental data were analyzed using the unpaired Student's t test. *$p \leq 0.05$, **$p \leq 0.01$. All results are expressed as mean ± SD. All error bars represent the standard deviations.

ASSOCIATED CONTENT

Supporting Information

The Supporting Information is available free of charge on the ACS Publications website at DOI: 10.1021/acsnano.9b02845.

Mechanical test, XRD patterns, HRTEM images (PDF)
Supporting movie (MP4)
Supporting movie (MP4)
Supporting movie (MP4)
Supporting movie (MP4)

AUTHOR INFORMATION

Corresponding Authors

*E-mail: yanglu@hfut.edu.cn.
*E-mail: taohe@hfut.edu.cn.

ORCID

Jingzhe Xue: 0000-0003-1171-2487
Zhengbao Zha: 0000-0003-3646-4969
Haisheng Qian: 0000-0003-4903-3447
Xinglong Gong: 0000-0001-6997-9526
Yang Lu: 0000-0002-8412-809X

Author Contributions

Y.L. and T.H. conceived the idea and supervised the project. W.W.F. synthesized polymers and characterizations. X.Y. prepared composite hydrogels and biorelated experiments. J.X., T.C.S., L.D., Z.Z., H.Q., Y.H.S., M.Z., and X.G. assisted with the experiments and characterizations. T.H., Y.L., W.W.F., and Y.X. cowrote the manuscript. All authors discussed the results and commented on the manuscript. All authors have given approval to the final version of the manuscript.

Author Contributions

#X.Y. and W.W.F. contributed equally.

Notes

The authors declare no competing financial interest.

ACKNOWLEDGMENTS

This work was financially supported by the National Natural Science Foundation of China (Nos. 51572067, 21574035, 21501039, 51702309), the Fundamental Research Funds for the Central Universities (No. JZ2018HGPA0269), the Anhui Provincial Natural Science Foundation (1708085ME114), and China Postdoctoral Science Foundation (2017M612079). We also thank Prof. Xiaoyuan Song in the Laboratory of Transcriptional Regulation in Senescence and Brain Aging

DOI: 10.1021/acsnano.9b02845
ACS Nano 2019, 13, 10074−10084

(University of Science & Technology of China, China) for providing NIH-3T3 cells.

REFERENCES

(1) Peppas, N. A.; Hilt, J. Z.; Khademhosseini, A.; Langer, R. Hydrogels in Biology and Medicine: From Molecular Principles to Bionanotechnology. *Adv. Mater.* **2006**, *18*, 1345−1360.

(2) Lee, J. B.; Peng, S.; Yang, D.; Roh, Y. H.; Funabashi, H.; Park, N.; Rice, E. J.; Chen, L.; Long, R.; Wu, M.; Luo, D. A Mechanical Metamaterial Made from a DNA Hydrogel. *Nat. Nanotechnol.* **2012**, *7*, 816−820.

(3) Zhou, Y.; Damasceno, P. F.; Somashekar, B. S.; Engel, M.; Tian, F.; Zhu, J.; Huang, R.; Johnson, K.; McIntyre, C.; Sun, K.; Yang, M.; Green, P. F.; Ramamoorthy, A.; Glotzer, S. C.; Kotov, N. A. Unusual Multiscale Mechanics of Biomimetic Nanoparticle Hydrogels. *Nat. Commun.* **2018**, *9*, 181.

(4) Hou, X.; Zhang, Y. S.; Santiago, G. T.-d.; Alvarez, M. M.; Ribas, J.; Jonas, S. J.; Weiss, P. S.; Andrews, A. M.; Aizenberg, J.; Khademhosseini, A. Interplay Between Materials and Microfluidics. *Nat. Rev. Mater.* **2017**, *2*, 17016.

(5) Feig, V. R.; Tran, H.; Lee, M.; Bao, Z. Mechanically Tunable Conductive Interpenetrating Network Hydrogels That Mimic the Elastic Moduli of Biological Tissue. *Nat. Commun.* **2018**, *9*, 2740.

(6) Song, P.; Qin, H.; Gao, H.-L.; Cong, H.-P.; Yu, S.-H. Self-healing and Superstretchable Conductors from Hierarchical Nanowire Assemblies. *Nat. Commun.* **2018**, *9*, 2786.

(7) Yuk, H.; Lin, S.; Ma, C.; Takaffoli, M.; Fang, N. X.; Zhao, X. Hydraulic Hydrogel Actuators and Robots Optically and Sonically Camouflaged in Water. *Nat. Commun.* **2017**, *8*, 14230.

(8) Liu, J.; Pang, Y.; Zhang, S.; Cleveland, C.; Yin, X.; Booth, L.; Lin, J.; Lucy Lee, Y. A.; Mazdiyasni, H.; Saxton, S.; Kirtane, A. R.; Erlach, T. V.; Rogner, J.; Langer, R.; Traverso, G. Triggerable Tough Hydrogels for Gastric Resident Dosage Forms. *Nat. Commun.* **2017**, *8*, 124.

(9) Sun, J.-Y.; Zhao, X.; Illeperuma, W. R. K.; Chaudhuri, O.; Oh, K. H.; Mooney, D. J.; Vlassak, J. J.; Suo, Z. Highly Stretchable and Tough Hydrogel. *Nature* **2012**, *489*, 133−136.

(10) Rauner, N.; Meuris, M.; Zoric, M.; Tiller, J. C. Enzymatic Mineralization Generates Ultrastiff and Tough Hydrogels with Tunable Mechanics. *Nature* **2017**, *543*, 407−410.

(11) Qin, H.; Zhang, T.; Li, H.-N.; Cong, H. P.; Antonietti, M.; Yu, S.-H. Dynamic Au-Thiolate Interaction Induced Rapid Self-Healing Nanocomposite Hydrogels with Remarkable Mechanical Behaviors. *Chem.* **2017**, *3*, 691−705.

(12) Kong, W.; Wang, C.; Jia, C.; Kuang, Y.; Pastel, G.; Chen, C.; Chen, G.; He, S.; Huang, H.; Zhang, J.; Wang, S.; Hu, L. Muscle-Inspired Highly Anisotropic, Strong, Ion-Conductive Hydrogels. *Adv. Mater.* **2018**, *30*, 1801934.

(13) Qu, J.; Zhao, X.; Liang, Y.; Xu, Y.; Ma, P. X.; Guo, B. Degradable Conductive Injectable Hydrogels as Novel Antibacterial, Anti-Oxidant Wound Dressings for Wound Healing. *Chem. Eng. J.* **2019**, *362*, 548−560.

(14) Liang, Y.; Zhao, X.; Hu, T.; Chen, B.; Yin, Z.; Ma, P. X.; Guo, B. Adhesive Hemostatic Conducting Injectable Composite Hydrogels with Sustained Drug Release and Photothermal Antibacterial Activity to Promote Full-Thickness Skin Regeneration During Wound Healing. *Small* **2019**, *15*, 1900046.

(15) Qu, J.; Zhao, X.; Liang, Y.; Zhang, T.; Ma, P. X.; Guo, B. Antibacterial Adhesive Injectable Hydrogels with Rapid Self-Healing, Extensibility and Compressibility as Wound Dressing for Joints Skin Wound Healing. *Biomaterials* **2018**, *183*, 185−199.

(16) Li, J.; Mooney, D. J. Designing Hydrogels for Controlled Drug Delivery. *Nat. Rev. Mater.* **2016**, *1*, 16071.

(17) Liu, X.; Steiger, C.; Lin, S.; Parada, G. A.; Liu, J.; Chan, H. F.; Yuk, H.; Phan, N. V.; Collins, J.; Tamang, S.; Traverso, G.; Zhao, X. Ingestible Hydrogel Device. *Nat. Commun.* **2019**, *10*, 493.

(18) Madl, C. M.; Heilshorn, S. C.; Blau, H. M. Bioengineering Strategies to Accelerate Stem Cell Therapeutics. *Nature* **2018**, *557*, 335−342.

(19) Bassat, E.; Mutlak, Y. E.; Genzelinakh, A.; Shadrin, I. Y.; Baruch Umansky, K.; Yifa, O.; Kain, D.; Rajchman, D.; Leach, J.; Riabov Bassat, D.; Udi, Y.; Sarig, R.; Sagi, I.; Martin, J. F.; Bursac, N.; Cohen, S.; Tzahor, E. The Extracellular Matrix Protein Agrin Promotes Heart Regeneration in Mice. *Nature* **2017**, *547*, 179−184.

(20) Xia, L.-W.; Xie, R.; Ju, X.-J.; Wang, W.; Chen, Q.; Chu, L.-Y. Nano-Structured Smart Hydrogels with Rapid Response and High Elasticity. *Nat. Commun.* **2013**, *4*, 2226.

(21) Li, Y.; Kumacheva, E. Hydrogel Microenvironments for Cancer Spheroid Growth and Drug Screening. *Sci. Adv.* **2018**, *4*, No. eaas8998.

(22) Li, S.; Dong, S.; Xu, W.; Tu, S.; Yan, L.; Zhao, C.; Ding, J.; Chen, X. Antibacterial Hydrogels. *Adv. Sci.* **2018**, *5*, 1700527.

(23) Zhao, X.; Guo, B. L.; Wu, H.; Liang, Y. P.; Ma, P. X. Injectable Antibacterial Conductive Nanocomposite Cryogels with Rapid Shape Recovery for Noncompressible Hemorrhage and Wound Healing. *Nat. Commun.* **2018**, *9*, 2784.

(24) Guo, B.; Ma, P. X. Conducting Polymers for Tissue Engineering. *Biomacromolecules* **2018**, *19*, 1764−1782.

(25) Konieczynska, M. D.; Villa-Camacho, J. C.; Ghobril, C.; Perez-Viloria, M.; Tevis, K. M.; Blessing, W. A.; Nazarian, A.; Rodriguez, E. K.; Grinstaff, M. W. On-Demand Dissolution of a Dendritic Hydrogel-based Dressing for Second-Degree Burn Wounds through Thiol-Thioester Exchange Reaction. *Angew. Chem., Int. Ed.* **2016**, *55*, 9984−9987.

(26) Yang, Y.; Zhang, J.; Liu, Z.; Lin, Q.; Liu, X.; Bao, C.; Wang, Y.; Zhu, L. Tissue-Integratable and Biocompatible Photogelation by the Imine Crosslinking Reaction. *Adv. Mater.* **2016**, *28*, 2724−2730.

(27) Moon, H. J.; Ko du, Y.; Park, M. H.; Joo, M. K.; Jeong, B. Temperature-responsive Compounds as *In situ* Gelling Biomedical Materials. *Chem. Soc. Rev.* **2012**, *41*, 4860−4883.

(28) Bouten, P. J.; Zonjee, M.; Bender, J.; Yauw, S. T.; van Goor, H.; van Hest, J. C.; Hoogenboom, R. The Chemistry of Tissue Adhesive Materials. *Prog. Polym. Sci.* **2014**, *39*, 1375−1405.

(29) Li, P.; Poon, Y. F.; Li, W.; Zhu, H.-Y.; Yeap, S. H.; Cao, Y.; Qi, X.; Zhou, C.; Lamrani, M.; Beuerman, R. W.; Kang, E.-T.; Mu, Y.; Li, C. M.; Chang, M. W.; Leong, S. S.; Chan-Park, M. B. A Polycationic Antimicrobial and Biocompatible Hydrogel with Microbe Membrane Suctioning Ability. *Nat. Mater.* **2011**, *10*, 149−156.

(30) Ghobril, C.; Grinstaff, M. W. The Chemistry and Engineering of Polymeric Hydrogel Adhesives for Wound Closure: A Tutorial. *Chem. Soc. Rev.* **2015**, *44*, 1820−1835.

(31) Bhatia, S. K. Traumatic Injuries. In *Biomaterials for Clinical Applications*; Springer: New York, 2010; pp 213−258.

(32) Jeong, B.; Kim, S. W.; Bae, Y. H. Thermosensitive Sol-Gel Reversible Hydrogels. *Adv. Drug Delivery Rev.* **2012**, *64*, 154−162.

(33) Li, L.; Yan, B.; Yang, J.; Chen, L.; Zeng, H. Novel Mussel-Inspired Injectable Self-Healing Hydrogel with Anti-Biofouling Property. *Adv. Mater.* **2015**, *27*, 1294−1299.

(34) DeLeo, F. R.; Otto, M.; Kreiswirth, B. N.; Chambers, H. F. Community-Associated Meticillin-Resistant *Staphylococcus Aureus*. *Lancet* **2010**, *375*, 1557−1568.

(35) Talan, D. A.; Mower, W. R.; Krishnadasan, A.; Abrahamian, F. M.; Lovecchio, F.; Karras, D. J.; Steele, M. T.; Rothman, R. E.; Hoagland, R.; Moran, G. J. Trimethoprim-Sulfamethoxazole Versus Placebo for Uncomplicated Skin Abscess. *N. Engl. J. Med.* **2016**, *374*, 823−832.

(36) Mao, C.; Xiang, Y.; Liu, X.; Cui, Z.; Yang, X.; Yeung, K. W. K.; Pan, H.; Wang, X.; Chu, P. K.; Wu, S. Photo-Inspired Antibacterial Activity and Wound Healing Acceleration by Hydrogel Embedded with Ag/Ag@AgCl/ZnO Nanostructures. *ACS Nano* **2017**, *11*, 9010−9021.

(37) Zhu, C.-H.; Lu, Y.; Peng, J.; Chen, J.-F.; Yu, S.-H. Photothermally Sensitive Poly(N-isopropylacrylamide)/Graphene Oxide Nanocomposite Hydrogels as Remote Light-Controlled Liquid Microvalves. *Adv. Funct. Mater.* **2012**, *22*, 4017−4022.

(38) Zhao, X.; Wu, H.; Guo, B.; Dong, R.; Qiu, Y.; Ma, P. X. Antibacterial Anti-Oxidant Electroactive Injectable Hydrogel as Self-Healing Wound Dressing with Hemostasis and Adhesiveness for Cutaneous Wound Healing. *Biomaterials* **2017**, *122*, 34−47.

DOI: 10.1021/acsnano.9b02845
ACS Nano 2019, 13, 10074−10084

(39) You, C.; Han, C.; Wang, X.; Zheng, Y.; Li, Q.; Hu, X.; Sun, H. The Progress of Silver Nanoparticles in The Antibacterial Mechanism, Clinical Application and Cytotoxicity. *Mol. Biol. Rep.* **2012**, *39*, 9193−9201.
(40) Gurtner, G. C.; Werner, S.; Barrandon, Y.; Longaker, M. T. Wound Repair and Regeneration. *Nature* **2008**, *453*, 314−321.
(41) Dong, R.; Zhu, B.; Zhou, Y.; Yan, D.; Zhu, X. Breathing" Vesicles with Jellyfish-like On-Off Switchable Fluorescence Behavior. *Angew. Chem., Int. Ed.* **2012**, *51*, 11633−11637.
(42) Xu, W.-P.; Zhang, L.-C.; Li, J.-P.; Lu, Y.; Li, H.-H.; Ma, Y.-N.; Wang, W.-D.; Yu, S.-H. Facile Synthesis of Silver@Graphene Oxide Nanocomposites and Their Enhanced Antibacterial Properties. *J. Mater. Chem.* **2011**, *21*, 4593−4597.
(43) Hu, B.; Wang, S.-B.; Wang, K.; Zhang, M.; Yu, S.-H. Microwave-Assisted Rapid Facile "Green" Synthesis of Uniform Silver Nanoparticles: Self-Assembly into Multilayered Films and Their Optical Properties. *J. Phys. Chem. C* **2008**, *112*, 11169−11174.
(44) Liu, K.; Dong, L.; Xu, Y.; Yan, X.; Li, F.; Lu, Y.; Tao, W.; Peng, H.; Wu, Y.; Su, Y.; Ling, D.; He, T.; Qian, H.; Yu, S.-H. Stable Gadolinium Based Nanoscale Lyophilized Injection for Enhanced MR Angiography with Efficient Renal Clearance. *Biomaterials* **2018**, *158*, 74−85.

DOI: 10.1021/acsnano.9b02845
ACS Nano 2019, 13, 10074−10084